

© 2015 IEEE. Personal use of this material is permitted. Permission from IEEE must be obtained for all other uses, in any current or future media, including reprinting/republishing this material for advertising or promotional purposes, creating new collective works, for resale or redistribution to servers or lists, or reuse of any copyrighted component of this work in other works.

Digital Object Identifier (DOI): 10.1109/ECCE.2015.7309959

Energy Conversion Congress and Exposition (ECCE), 2015 IEEE, September 2015

**Thermal stress reduced maximum power point tracking for two stages photovoltaic converters**

Markus Andresen  
Giampaolo Buticchi  
Marco Liserre

**Suggested Citation**

M. Andresen, G. Buticchi and M. Liserre, "Thermal stress reduced maximum power point tracking for two stages photovoltaic converters," *2015 IEEE Energy Conversion Congress and Exposition (ECCE)*, Montreal, QC, 2015, pp. 2116-2123.

# Thermal Stress Reduced Maximum Power Point Tracking for Two Stages Photovoltaic Converters

Markus Andresen, Giampaolo Buticchi, Marco Liserre  
Christian-Albrechts-Universität zu Kiel,  
Chair of Power Electronics  
Kiel, Germany  
{ma,gibu,ml}@tf.uni-kiel.de

**Abstract**— Several maximum power point tracking (MPPT) methods have been proposed to optimize the energy harvesting of photovoltaic systems. However, the optimization of the energy harvesting can produce extremely variable loading of the power semiconductors resulting in a decrease of the system lifetime. This work proposes a multi-objective MPPT for two-stage photovoltaic converters, where the semiconductor thermal stress is taken into account while searching for the maximum power point. A perturb and observe based algorithm which limits the positive temperature gradient and the maximum junction temperature of the power semiconductors is introduced and fully validated in the laboratory with a mission profile emulating variable irradiance conditions.

**Keywords**— *Maximum power point tracking; reliability; thermal cycling; PV systems*

## I. INTRODUCTION

Photovoltaic power plants are built worldwide to increase the renewable energy production and power electronics are a key factor for their grid integration [1]. To amortize their high manufacturing costs, these systems need to harvest maximum power for lifetimes of 20 years. Among the most sensitive components are the power semiconductors, which are prone to failure. The underlying aging mechanism of the power semiconductors is thermal cycling, which causes mechanical stress between materials with different coefficients of thermal extension [2],[3],[4]. For Photovoltaic (PV) power plants, several power converter topologies have been introduced, which have different benefits in terms of efficiency, current ripple or leakage current [5]. Moreover, algorithms for harvesting the maximum power for the PV arrays have been presented [6],[7]. The strategies offer different advantages with respect to tracking speed, complexity and performance under partial shading conditions. The maximization of the energy harvesting is important to justify the cost of a PV system. However, the possible failure of the power converter is also impacting the cost of PV energy. As a matter of fact, a MPPT strategy that takes into account the increased costs due to low reliability would help optimizing the investments of the PV systems.

A reduction of thermal cycling for the power semiconductors increases the reliability of the system [8]. In

literature an analysis is done for the reliability critical parts of the photovoltaic system [9]. The reliability of several components, different Maximum Power Point Tracking (MPPT) algorithms and anti island schemes is evaluated, but no action is taken to improve the algorithms with respect to reliability.

This work proposes to apply a “lifetime-corrected” MPPT to control the stress of the power electronics in the DC/DC converter. The thermal effects of traditional MPPT algorithms are analyzed and an algorithm is introduced, which reduces the thermal stress during fast changing irradiance and limits the maximum junction temperature.

The algorithm relies on a feedback of the junction temperature. In this initial work the temperature is directly measured on the chip surface with a wide-bandwidth temperature measurement instrument to validate the principle. For future works, several methods including the use of Thermo Sensitive Electrical Parameter (TSEP) [10] or junction temperature observers [11] will be used instead of the high speed measurement system in order to make this solution cost-effective.

In section II an introduction in reliability issues of power electronic modules is given, while section III analyses the problem of fast changing irradiance in combination with MPPT for two stages PV systems. Section IV describes the proposed modified MPPT algorithm and in section V the laboratory setup is presented together with tests of the steady state and the dynamical behavior of the algorithm. The experimental analysis of the tradeoff between lifetime consumption and maximum harvested energy is analyzed in section VI. Finally, in section VII the results are summarized.

## II. RELIABILITY IN POWER ELECTRONICS

Power electronics are often assembled in power electronic modules for improved heat transfer capability and for increased power density. In these modules, the chips are mounted on multi layer configurations, called direct bonded copper (DBC), to ensure the electrical insulation and good heat dissipation [12]. Thereby the chips are soldered on the DBC, which consists of a substrate enclosed by two separated layers of copper. Beside the low heat transfer capability of the substrate compared to copper, these materials have unequal

coefficients of thermal extension (CTE). The resulting problem is the strain between the layers caused by temperature gradients and variations in the temperature. This strain is regarded as the main reason for aging of power electronic modules in literature and has led to significant effort to overcome the reliability issues and to monitor the degradation [13]. Consequently, to increase the lifetime of the power semiconductors, either the interconnections between the different layers with CTE-mismatch have to be improved or the thermal cycles need to be reduced. A problem often addressed by the manufacturers is the interconnection between the semiconductors. The state of the art bond wires lift off in case of a soldered connection. This is can be improved with sintered connections, but heel cracking remains a common failure [14]. Another problem is solder fatigue, which either occurs between the chip and the DBC or between the DBC and the baseplate. This reduces the heat transfer capability, which results in higher junction temperatures and finally in a failure [15]. For protection against corrosion and environmental influences, a gel filling immerses the module to guarantee dielectric strength. The main aging processes of this silicone gel are water trees, partial discharge and electrical trees, which are degrading effects causing aging but not the destruction [16]. Beside the failures caused by degradation, there are further potential reasons for failures caused by the environment, such as cosmic rays [17], vibration and humidity [14].

The lifetime estimation of power electronics is a challenging topic, because of the various different influences and possible failure mechanisms. In this area the physics of failure analysis is nowadays established [3]. However, a simple model for the lifetime estimation is the Coffin-Manson equation (1).

$$N_f = a \cdot (\Delta T_j)^{-n} \quad (1)$$

It can be seen that the number of cycles to failure  $N_f$  depends exponentially on the magnitude of the thermal cycles  $\Delta T_j$ . The coefficients  $a$  and  $n$  are constants, which are empirically obtained. Despite the simple form of the equation, the exponential dependence of the thermal cycles is also shown in many lifetime models of failure mechanisms [18] presented in literature. To obtain the magnitude of the thermal cycles  $\Delta T_j$ , Rainflow counting [19] is usually applied for the junction temperature profile. The potential of Rainflow counting lies in the extraction of the time independent cycles from a mission profile. Despite the availability of several counting algorithms, Rainflow counting is most applied in reliability research, because it extracts the highest magnitudes from a profile, even though they are superposed by further smaller cycles.

The obtained thermal cycles are used in a parameterized lifetime model to investigate the reliability. A possible parameterization can be extracted by linear interpolation of the LESIT results [20], which were obtained by accelerated lifetime tests. This model is described with (2), whereby  $T_{j,mean}$  defines the average temperature of a thermal cycle  $\Delta T_j$ .

$$N_f = 4.48 \cdot 10^{14} \cdot (\Delta T_j)^{-5.024} \cdot e^{(-T_{j,mean}+77.5) \cdot 0.0555} \quad (2)$$

This lifetime model defines the number of thermal cycles to failure  $N_f$  for a singular magnitude. Since a real mission profile contains several thermal cycles with different magnitudes, the damage needs to be accumulated, which can be done with the Palmgren-Miners rule (3) [21], where  $N_i$  is the lifetime for the stress range  $i$  and  $n_i$  is the actual number of applied stress range  $I$  (2). As  $c \geq 1$ , the device fails.

$$\sum_{i=1}^k \frac{n_i}{N_i} = c \quad (3)$$

This linear extrapolated lifetime model is known to lack of precision, but still it indicates the mathematical connection to the failure mechanisms, such as bond wire liftoff and solder fatigue.

### III. THERMAL STRESS OF MAXIMUM POWER POINT TRACKING

In photovoltaic systems the main goal is to harvest the maximum available energy from the array. To extend the operation range, often a boost converter is used to step-up the voltage to the level of the DC link voltage. At the same time, the boost converter implements the MPPT algorithm. The structure of a two-stage PV system with two parallel boost converters is shown in Fig. 1. The MPPT in this work is performed by control of the duty cycle  $d$ , which is expressed by the ratio of the turn on time of the IGBT  $t_{on}$  and the sampling time  $T_s$  or with the PV array voltage  $U$  and the DC-link voltage  $U_{dc}$  as shown in (4).

$$d = \frac{t_{on}}{T_s} = 1 - \frac{U}{U_{dc}} \quad (4)$$

To perform MPPT, the controller needs to have information about the current operation point and at least the current and voltage measurements of one additional operation point. The excitation of the system to obtain these measurements causes thermal stress for the power electronics. This excitation depends on the MPPT algorithm, which normally implies the

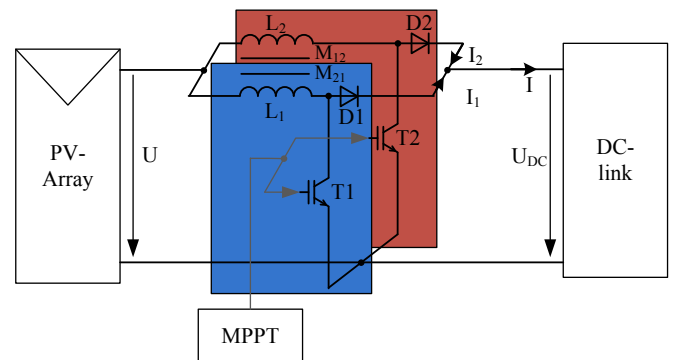


Fig. 1. DC/DC converter of a two stage photovoltaic system.

control of the current or voltage of the PV array. The optimal point of operation is changing with the irradiance and thus over the time. On days with fast passing clouds, the irradiance is varying fast and thus the optimal set point for the MPPT changes, too [22]. The passing clouds cause power cycling for the power semiconductors and thus cause additional thermal cycles of the junction temperature, which reduces their lifetime.

To evaluate the relevance of the varying irradiance and its impact on semiconductor's lifetime, in Fig. 2 the irradiance is measured and displayed for one day in 1 min average values. The sun is rising before 6 am and increases the irradiance until its maximum around 11:45 until it sunset at approximately 18:30. The irradiance is rapidly changing with various different magnitudes and time periods during the whole day. To better identify the cycles in the profile, Rainflow counting is applied and presented in Fig. 3 in dependence of the irradiance cycle and the time period of the cycle. In the profile, it can be seen that different magnitudes of irradiance are well distributed in the profile, while the relatively short time periods with less than one hour are predominant.

In literature many MPPT algorithms can be found, whereby most of them can be categorized in the following basic schemes:

- Open voltage measurement or short circuit current measurement
- Curve sweeping
- Perturb & Observe (P&O) or incremental conductance

These algorithms have advantages and disadvantages with respect to tracking speed, detection of partial shading conditions or thermal stress for the power semiconductors. Concerning the thermal stress, short circuit current measurement is known to be problematic for the lifetime of the system. To overcome a disadvantage of one scheme, algorithms can be combined e.g. [7]. But not only the advantages sum up: also the disadvantages, such as thermal

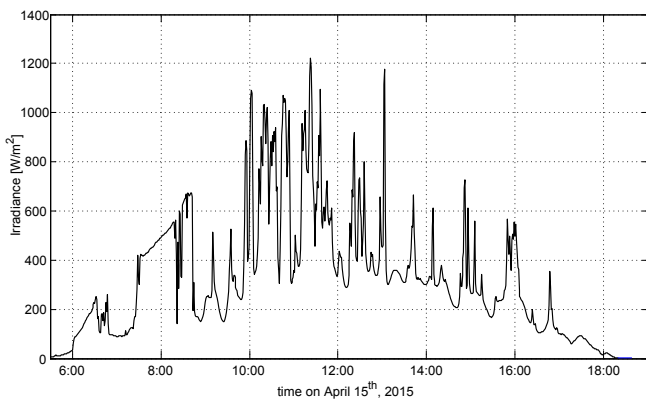


Fig. 2. Measured irradiance on April 15<sup>th</sup>, 2015 in Colorado at NFEL Solar Radiation Laboratory [23].

stress of short circuit current measurement needs to be considered.

The thermal stress of the three above mentioned MPPT algorithms can be analyzed theoretically. The measurement of the open circuit voltage ( $d = 0$ ) or the short circuit current ( $d = 1$ ), causes a variation of thermal stress and thus thermal cycling. Worst from the point of thermal stress is curve sweeping, because the whole curve from  $d=0...1$  is passed through for the MPPT and thus minimum load and maximum load is applied every time the algorithm is run, leading to significant stress. Instead, when the P&O algorithm is operating in the MPP, only low thermal stress is expected during constant irradiance. Thus among the considered MPPT strategies, the P&O is expected to be the best from the point of thermal stress. Other algorithms behave in a similar way and avoid large power swings.

#### IV. "LIFETIME-CORRECTED" MPPT

In the following, the P&O algorithm will be used as a base for the thermal stress control due to its wide use in PV converters. In Fig. 4 the conditions are shown, in which the thermal stress reduction is applied. During fast changing radiation a positive temperature gradient limitation  $\Delta T_{j,max}$  is applied and for high load operation a maximum junction temperature limitation  $T_{j,max}$  is implemented. These targets can be set at the same time without conflicting with each other. The first goal to reduce thermal cycling during fast changing

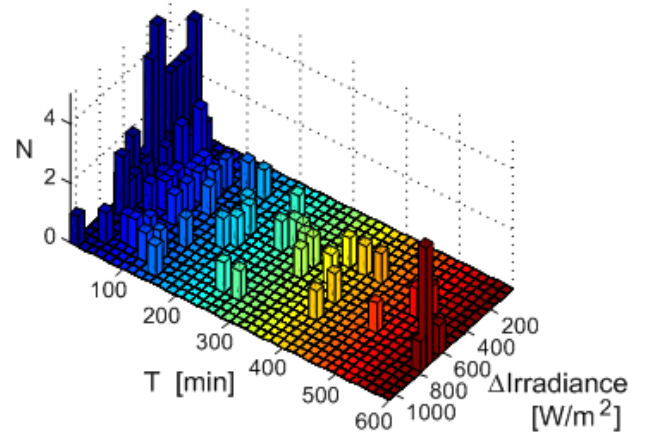


Fig. 3. Rainflow counted thermal cycles in dependence of irradiance and time period of the irradiance profile in Fig. 2.

irradiance is implemented by limiting the positive temperature gradient at the price of a slower and less energy efficient MPPT. The gradient is chosen because of the unpredictable

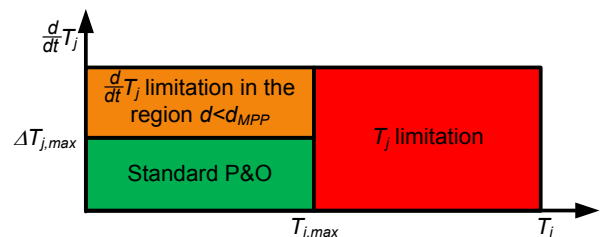


Fig. 4. Regions for application thermal stress reduction.

behavior of passing clouds, which reduce the irradiance in fast changing weather conditions. In case of a shaded PV array and dispersing clouds, it is not certain how long it takes until the next cloud shadows the array. The temperature gradient limitation shows the advantage not to influence the operation on a sunny day for an adequate temperature gradient  $\Delta T_{j,max}$ , but prevents excessive thermal swings during fast changing irradiance.

The second control target, the limitation of the maximum junction temperature  $T_{j,max}$ , is used to achieve maximum utilization of the power semiconductors, by guaranteeing not to exceed the maximum junction temperature. This mechanism enables de-rating of the components, which reduces system costs. A flow chart shows the realization of the overall MPPT based on the P&O algorithm in Fig. 5. At the beginning of the algorithm, the electrical ( $U_{dc}$ ,  $I_k$  and  $P_k$ ) and thermal ( $T_{j,T}$  and  $T_{j,D}$ ) properties are sampled and updated. From the duty cycle and the dc-link voltage, the PV- array voltage can be derived as shown in (4).

temperature can vary before the controller limits the energy harvesting. An advantage of this scheme is low influence of the noise related to the temperature measurement during normal operation. The first condition of the MPPT algorithm is to check the temperature limitations. In case of a violation of the maximum temperature gradient or the maximum temperature,  $d$  is increased to reduce the output power. A high increase is made in the case of power point tracking in the current source region ( $d > d_{MPP}$ ) because of the reduced thermal stress in this region. If no temperature violation is detected, the normal P&O algorithm is carried out with the comparison of the power variation and the voltage variation. Additionally, the new thermal limitation for the next maximum temperature gradient limitation needs to be set. This part is independent from the power variation, but in the case of a temperature decrease, the new maximum temperature of the next step is set to the temperature given by the gradient limitation. Otherwise, for increasing temperatures, the new maximum temperature is the sum of the old maximum temperature and the applied

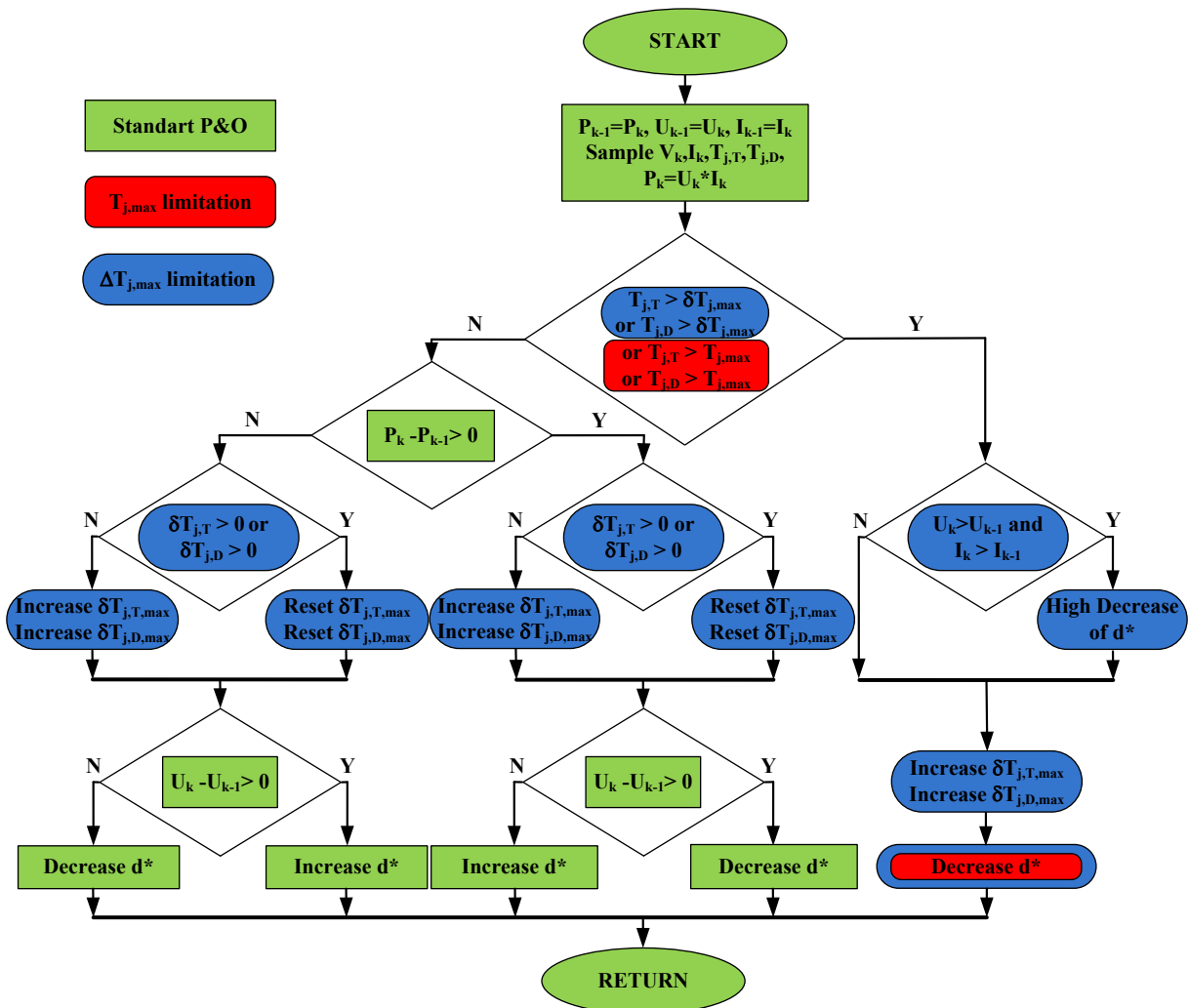


Fig. 5. Flow chart of the thermal stress and temperature limited maximum power point tracking algorithm.

The positive temperature gradient limitation is applied in region  $d < d_{MPP}$  by means of a tolerance band in which the

gradient. In (5) the mathematical expression is shown.

$$\delta T_{j,max} = \begin{cases} T_{j,max} + \Delta T_{j,max} \cdot T_{mppt} \frac{d}{dt} T_j(t) > 0 \\ T_j + \Delta T_{j,max} \cdot T_{mppt} \frac{d}{dt} T_j(t) < 0 \end{cases} \quad (5)$$

## V. TUNING OF THE PROPOSED MPPT ALGORITHM

To demonstrate the effectiveness of the proposed MPPT algorithm, the behavior is tested in three different conditions:

- Steady-state operation
- A step-variation in the overall maximum junction temperature
- The temperature gradient limitation for a high increase in the irradiance.

The influence of the MPPT on the thermal stress is tested on a PV system with boost inverter in continuous current conduction mode. A PV emulator is used to emulate the PV array and the boost converter is operated in interleaved mode.

TABLE I. SYSTEM PARAMETERS

Variable	Switching frequency $f_s$	Irradiation	$U_{dc}$	$L_1=L_2$ $=M_{12}$ $=M_{21}$	$U_{oc}$	$I_{sc}$
Value	15 kHz	1 kW/m <sup>2</sup>	380 V	3 mH	180 V	10 A

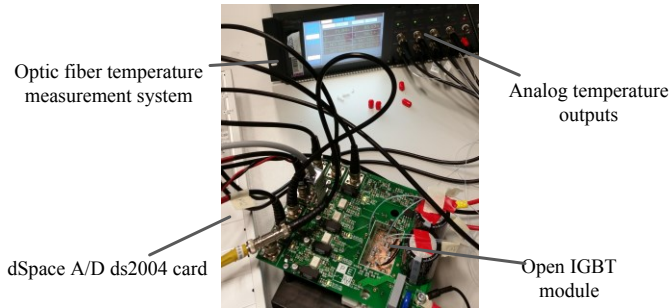


Fig. 6. Picture of the laboratory setup.

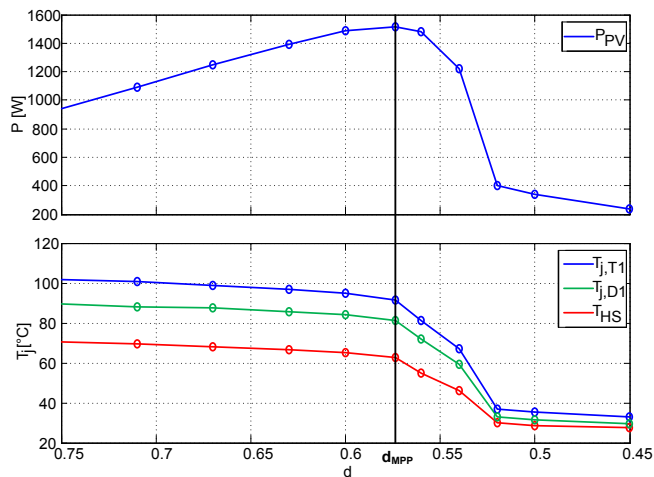


Fig. 7. Measured PV output power and junction temperature of the power semiconductors of the boost converter for varying duty cycles and constant irradiance.

The system is shown in Fig. 6 with the parameters of Table I. The maximum power point is set to  $U_{MPP} = 160 V$  and  $I_{MPP}$

$= 9.5 A$ . In the boost converter a Danfoss (DP25H1200T101667-101667) open IGBT modules is used and the junction temperature measurement is done with a high bandwidth optic fiber measurement system, which is directly fed back into the used dSpace 1006 system. The dc-link is controlled by an electronic load. For thermal stress analysis, the junction temperature of the IGBT T1, the Diode D1 and one spot on the passive heat sink are measured and displayed in Fig. 7 with the parameters of Table I for a variation of the duty cycle  $d$ . The system is driven with each  $d$  until it reaches approximately steady-state conditions. This requires a substantial long time, because the heat sink needs a long time to reach thermal steady-state. Remarkably, the Maximum Power Point (MPP) with the duty cycle  $d_{MPP}$  is not the point with the maximum temperature for the power semiconductors. The thermal stress increases with an increase of the duty cycle, which can be explained with an increase of the current ripple and a decrease in the DC part, which leads to a lower root mean square value of the current. Thus the current ripple needs to be minimized in operation, which is achieved in the MPP. In general, the diode is colder than the IGBT and the temperature difference between the power semiconductors and the heat sink temperature increases with the temperature of the power semiconductors. Furthermore, the operation points with equal power transfer for  $d > d_{MPP}$  are more stressing than for  $d < d_{MPP}$ . The heat sink temperature even reaches a  $70^\circ C$  compared to  $62^\circ C$  in the MPP.

For demonstrating the effectiveness of the maximum temperature limitation, the system is operated without thermal limitations until it reaches thermal steady-state conditions for an MPPT period  $T_{MPPT} = 50 ms$ . This is shown in Fig. 8, where at  $t = 2 s$  the temperature limitation is changed from  $T_{j,max} = 110^\circ C$  to  $T_{j,max} = 85^\circ C$ . Displayed are the junction sink temperatures of one IGBT and one Diode, the heat

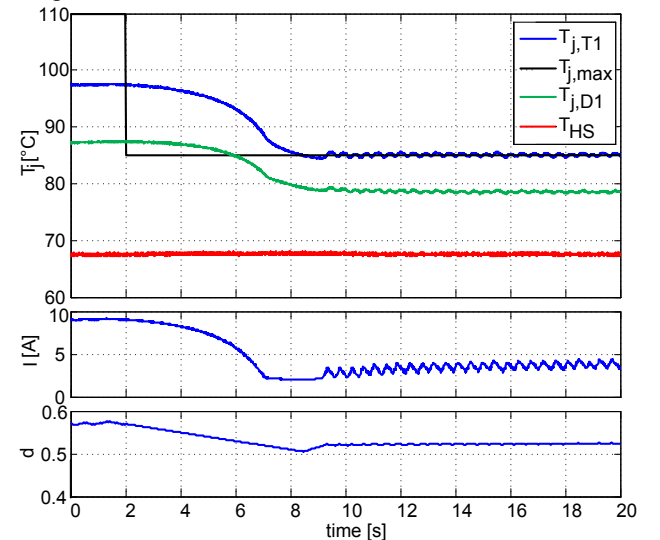


Fig. 8. Behavior of the MPPT for a step in the maximum junction temperature  $T_{j,max} = 110^\circ C \rightarrow T_{j,max} = 85^\circ C$  and  $T_{mppt} = 50 ms$ .

temperature, the array current and the duty cycle. The

maximum temperature reference step forces the MPPT to decrease the duty cycle, which at the same time reduces the PV current and thus the temperature. The cooling down can be seen for 6 s until  $t = 8$  s. Afterwards the duty cycle is increased again until the temperature limitation is violated. In steady-state this leads to an oscillation of the output power and a consequent oscillation of the junction temperatures, which can be seen in the profile of the currents  $I$ . This oscillation can be reduced by either reducing the step size of the MPPT or the execution period  $T_{mppt}$ . The disadvantage is a slower tracking of the MPP, which is undesired. The diode has a lower

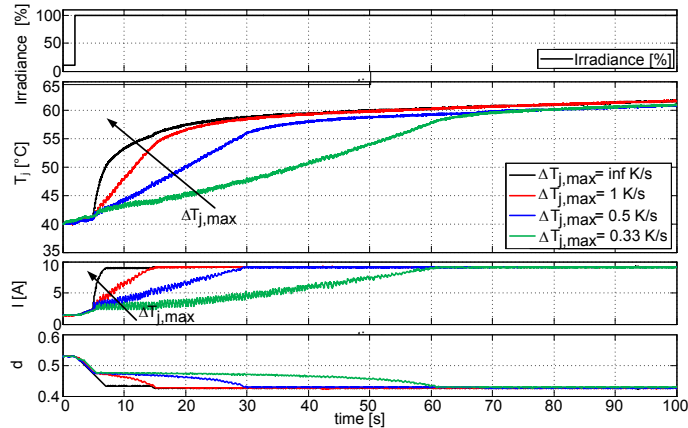


Fig. 9. Behavior of the MPPT for a step in the irradiance  $P_{PV,rel} = 10\% \rightarrow P_{PV,rel} = 100\%$  for different temperature gradients and normalized starting temperature in one IGBT.

temperature of the heat sink changes only marginally. Next, the junction temperature gradient limitation is tested. To achieve a sufficient increase in the temperature, the irradiance is set to  $P_{PV,rel} = 10\%$  and increased in a step to  $P_{PV,rel} = 100\%$ . This experiment is done without temperature gradient limitation and for  $\Delta T_{j,max} = \{1, 0.5, 0.33\} K/s$ . The results are shown in Fig. 9 for the junction temperature of the IGBT, which was discovered to reach the highest temperature in the boost converter. Without the gradient limitation, the MPPT directly detects the new maximum power point after 5 s, while the temperature of the IGBT is increasing quickly. The maximum temperature gradient limitation holds in all cases and the maximum power point is reached after 13 s, respectively 28 s and 58 s. Even if the most stringent temperature gradient limitation of  $\Delta T_{j,max} = 0.33$  K/s holds, the instantaneous increase of the temperature for an increase of the duty cycle is challenging the algorithm and sets the limit for the given experiment in the system, parameter tuning and measurement equipment.

## VI. LIFETIME ESTIMATION OF THE PROPOSED MPPT ALGORITHM

To evaluate the behavior of the controller during unpredictable changes in the irradiance, a 620 s mission profile is created and the thermal controller is tuned with the similar temperature gradients as in the previous experiment to investigate the tradeoff between reduced thermal stress and maximum power harvesting. Compared to the standard for MPPT profile testing [24], the irradiance profile is changed to

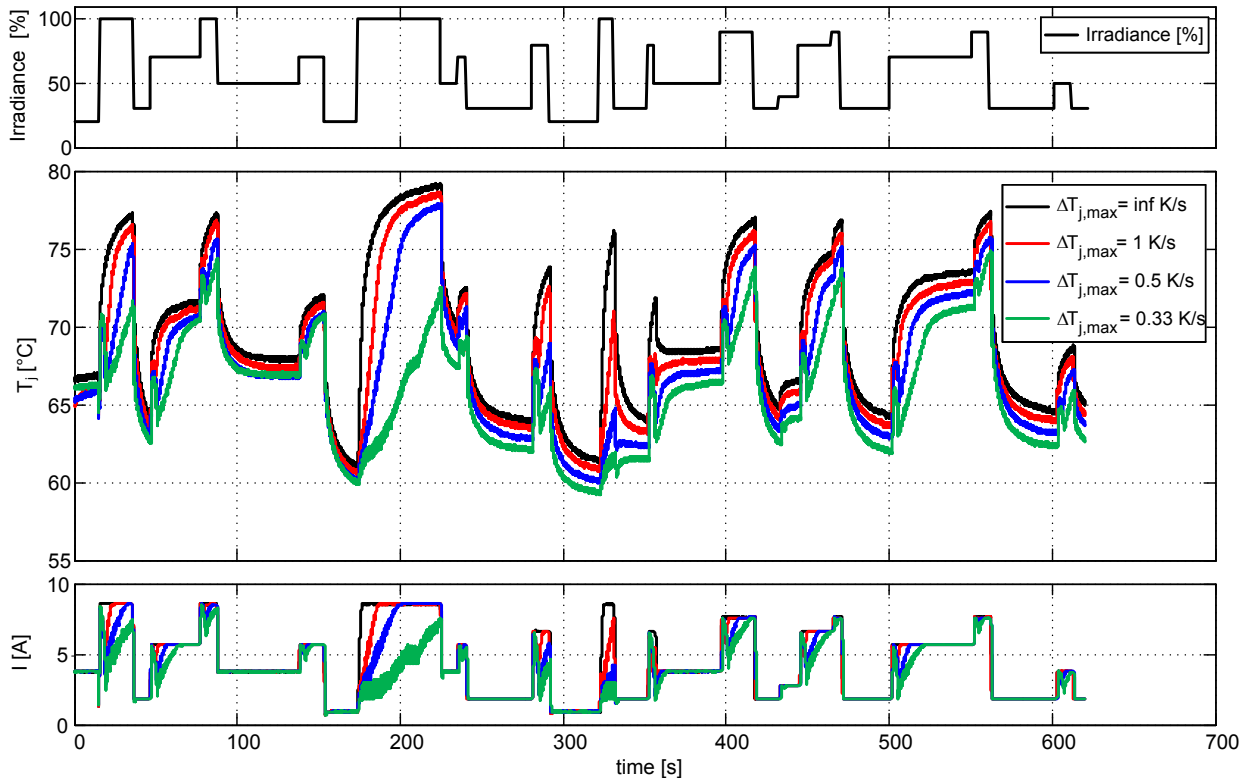


Fig. 10. Comparison of the MPPT for different temperature gradients during a 620 s mission profile with the parameters of Table I. temperature than the IGBT in the whole experiment and the have short ramp up/down times and different magnitudes and

time periods to see the behavior under different conditions. Standard trapezoidal MPPT testing profiles were not used because they would lead to a repetition of the temperature profiles, while the used profile shows the response to different variations in frequency and irradiation cycles. The profile is characterized by irradiance cycles with time periods of 4 s and 50 s, which is within the time affected by the thermal controller as shown in Fig. 9. Larger periods are not considered, because the thermal gradient limitations would not affect the long time system behavior. The mission profile, the junction temperatures of the IGBT and the currents of the profile are shown in Fig. 10 for the different junction temperature gradient limitations  $\Delta T_{j,max} = \{1, 0.5, 0.33\}$  K/s. Without the junction temperature gradient limitation, the current  $I$  is proportional to the irradiance profile, which shows good tracking of the maximum power point. The junction temperature of the IGBT shows the same shape, but low pass filtered. The activation of the temperature gradient limitation shows the expected behavior and the gradients are visible in the temperature profile. A problem of the short ramp up time of the rising irradiance can be seen in the inherent increase of the current  $I$ , which causes an uncontrolled increase of the IGBT junction temperature. The controller is reacting on this increase and affects a cool down, which consequently leads to a new thermal cycle with reduced magnitude. Such changes, however, should not be expected in a real application, and are used in this work to highlight the behavior of the proposed algorithm. A possible solution is to perform faster MPPT, which either calls for faster temperature sensors or an online temperature model. However, the temperature gradient

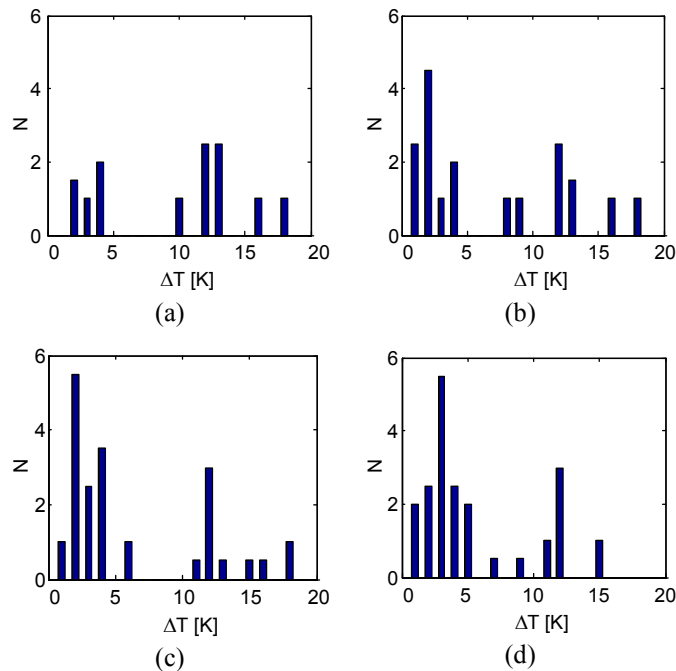


Fig. 11. Rainflow histogram of the mission profile in Fig. 9: (a)  $\Delta T_{j,max} = inf$ , (b)  $\Delta T_{j,max} = 1$ , (c)  $\Delta T_{j,max} = 0.5$ , (d)  $\Delta T_{j,max} = 0.33$ .

limitation holds and reduces the thermal swing of short

increases in irradiance, e.g. the thermal swing at  $t = 320$  s. Instead, long periods of irradiance changes are hardly affected, e.g. at  $t = 500$  s. To evaluate the achieved benefits and the costs for the MPPT algorithm, an estimation of the lifetime consumption needs to be made. The mathematical model of the LESIT results is used in combination with linear damage accumulation as described in (2)-(3). To identify the thermal cycles from the mission profile, Rainflow counting is applied. The histograms with 20 boxes with a width of 1 K for the thermal swings of all tunings are shown in Fig. 11.

The higher the magnitude of a cycle, the higher is its impact on the lifetime consumption. Without the temperature gradient limitation, the histogram shows one cycle for the magnitudes  $\Delta T = \{18, 16\}$  K and 2.5 cycles with a magnitude of  $\Delta T = \{12, 13\}$  K. Furthermore, there is one cycle at  $\Delta T = 10$  K and 5 cycles with a magnitude  $\Delta T < 5$  K. For the temperature gradient limitation  $\Delta T_{j,max} = 1$  K, the high magnitudes are remaining, but one cycle with a magnitude of  $\Delta T = 13$  K is reduced and a new cycle at  $\Delta T = 8$  K is new in the histogram. Caused by the implementation of the temperature gradient limitation in this work there are 10 cycles with a magnitude of  $\Delta T < 5$  K, which means there are five new thermal cycles with low magnitude. For the more stringent temperature gradient limitation, a better reduction of the thermal cycles with high magnitude is achieved. Especially, in the case of  $\Delta T_{j,max} = 0.33$  K a considerable shift from high magnitude thermal cycles to lower cycles is achieved. These results are basis for the derivation of the lifetime consumption of the different profiles. The results are collected in Table II, together with the derived average temperature of the different profiles and the energy harvested from the PV array. The harvested energy is derived with the measurement data of the dSpace System, which implies a certain inaccuracy of the relatively slow sampling rate compared to the dynamic of the currents. Similar, the thermal steady-state before the experiment is started might not be totally equal, leading to an imprecision of the average temperature. However, a limitation with  $\Delta T_{j,max} = 1$  K/s leads to a reduced average temperature by 1 K and only reduced energy production of 3.7 %, while the accumulated damage is only 89% of the case without temperature gradient limitation. Thus under the tested mission profile, the lifetime of the system would increase by 13 % compared to the system without temperature gradient limitation. For the more stringent limitations this trend is amplified, showing the tradeoff between maximum energy harvesting and increased lifetime. In the case of the highest temperature gradient limitation of  $\Delta T_{j,max} = 0.33$  K/s, the average temperature is decreased by 4.7 K and the energy production is reduced to 82,8% of its possible value, while the lifetime is increased by 189%. Despite the reduction of the harvested energy, it must be considered that the majority of the energy harvested by a PV system comes from sunny days, while the temperature gradient limitation affects the operation only during fast-changing irradiance conditions. As a matter of fact, while the total accumulated damage is greatly reduced, the loss in harvested power may not be so relevant, if the total useful life of the system is considered.

TABLE II. ANALYSIS OF THE MISSION PROFILE TESTS SHOWN IN FIG. 9 WITH DIFFERENT POSITIVE TEMPERATURE GRADIENTS.

	$\Delta T_{j,max} = \text{inf}$	$\Delta T_{j,max} = 1$	$\Delta T_{j,max} = 0.5$	$\Delta T_{j,max} = 0.33$
$T_{j,mean}$ [K]	69.5	68.5	67.3	67.3
$E_{total}$ [Wh] (rel.)	287.2 (1.0)	276.6 (96.31)	263.0 (91.57)	237.8 (82.80)
Acc. damage (rel.)	$7.16 \cdot 10^{-9}$ (1.0)	$6.35 \cdot 10^{-9}$ (0.89)	$5.46 \cdot 10^{-9}$ (0.76)	$2.48 \cdot 10^{-9}$ (0.35)
Rel. lifetime extension	1.0	1.13	1.31	2.89

## VII. CONCLUSION

Power electronics in photovoltaic systems are subjected to high thermal stress during fast changing irradiance, which is affecting their reliability. To overcome this problem, the thermal stress of different maximum power point tracking strategies for two stages PV power plants has been analyzed and hill climbing methods have found to cause least thermal stress for the power semiconductors. The perturb and observe algorithm has been extended with a limitation of the junction temperature gradient of the power semiconductors to reduce the thermal stress during fast changing irradiance. For a mission profile subjected to fast changing irradiance the tradeoff between energy harvesting and lifetime consumption is experimentally demonstrated. Reduced thermal stress and thus improved reliability of the power electronic components is achieved at the expense of reduced energy harvesting. Under tested conditions, a reduction of 3.7 % of the energy harvested has increased the lifetime for the investigated mission profile by 13 %.

## ACKNOWLEDGMENT

The research leading to these results has received funding from the European Research Council under the European Union's Seventh Framework Programme (FP/2007-2013) / ERC Grant Agreement n. 616344 – Heart.

## REFERENCES

- [1] R. Teodorescu, M. Liserre, P. Rodriguez, "Grid converters for photovoltaic and wind power systems," vol. 29, John Wiley & Sons, 2011.
- [2] Yi-Shao Lai, Tong Hong Wang, Chang-Chi Lee, "Thermal-Mechanical Coupling Analysis for Coupled Power- and Thermal-Cycling Reliability of Board-Level Electronic Packages," *IEEE Transactions on Device and Materials Reliability*, vol.8, no.1, pp.122-128, March 2008.
- [3] Huai Wang, M. Liserre, F. Blaabjerg, P. de Place Rimmen, J.B. Jacobsen, T. Kvisgaard, J. Landkildehus, "Transitioning to Physics-of-Failure as a Reliability Driver in Power Electronics," *IEEE Journal of Emerging and Selected Topics in Power Electronics*, vol.2, no.1, pp.97-114, March 2014.
- [4] M. Musallam, C. Yin, C. Bailey, M. Johnson, "Mission Profile-Based Reliability Design and Real-Time Life Consumption Estimation in Power Electronics," *IEEE Transactions on Power Electronics*, vol.30, no.5, pp.2601-2613, May 2015.
- [5] S.B. Kjaer, J.K. Pedersen, F. Blaabjerg, "A review of single-phase grid-connected inverters for photovoltaic modules," *IEEE Transactions on Industry Applications*, vol.41, no.5, pp.1292-1306, Sept.-Oct. 2005.
- [6] N. Femia, G. Petrone, G. Spagnuolo, M. Vitelli, "Power electronics and control techniques for maximum energy harvesting in photovoltaic systems," CRC Press, 2012.

- [7] J.S.C.M. Raj, A.E. Jeyakumar, "A Novel Maximum Power Point Tracking Technique for Photovoltaic Module Based on Power Plane Analysis of I-U Characteristics," *IEEE Transactions on Industrial Electronics*, vol.61, no.9, pp.4734-4745, Sept. 2014.
- [8] M. Andresen, M. Liserre, G. Buticchi, "Review of active thermal and lifetime control techniques for power electronic modules," 16th European Conference on Power Electronics and Applications (EPE'14-ECCE Europe), pp.1-10, 2014.
- [9] G. Petrone, G. Spagnuolo, R. Teodorescu, M. Veerachary, M. Vitelli, "Reliability Issues in Photovoltaic Power Processing Systems," *IEEE Transactions on Industrial Electronics*, vol.55, no.7, pp.2569-2580, 2008.
- [10] N. Baker, M. Liserre, Dupont, Y. Avenas, "Improved Reliability of Power Modules: A Review of Online Junction Temperature Measurement Methods," *IEEE Industrial Electronics Magazine*, vol.8, no.3, pp.17-27, Sept. 2014.
- [11] M. Musallam, C.M. Johnson, "Real-Time Compact Thermal Models for Health Management of Power Electronics," *IEEE Transactions on Power Electronics*, vol.25, no.6, pp.1416-1425, June 2010.
- [12] C. Busca, R. Teodorescu, F. Blaabjerg S. Munk-Nielsen, L. Helle, T. Abeyasekera, R. Rodriguez, "An overview of the reliability prediction related aspects of high power IGBTs in wind power applications," *Microelectronics Reliability*, vol. 51, pp. 1903-1907, Nov. 2011.
- [13] H. Oh, B. Han, P. McCluskey, C. Han, B.D. Youn, "Physics-of-Failure, Condition Monitoring, and Prognostics of Insulated Gate Bipolar Transistor Modules: A Review," *IEEE Transactions on Power Electronics*, vol. 30, no.5, pp. 2413-2426, (2015).
- [14] W. Ningyan, I. Cotton, K. Evans, "Impact of Thermal Cycling in Humid Environments on Power Electronic Modules," *IEEE Transactions on Components, Packaging and Manufacturing Technology*, vol. 2, pp. 1085-1091, July 2012.
- [15] Dawei X., Ran L., Tavner P., Shaoyong Y., Bryant A., Mawby P.: Condition Monitoring Power Module Solder Fatigue Using Inverter Harmonic Identification, *IEEE Transactions on Power Electronics*, vol. 27, pp. 235-247, Jan. 2012.
- [16] Fabian J.-H., Hartmann S., Hamidi A.: "Analysis of insulation failure modes in high power IGBT modules," *IEEE Industry Applications Conference*, Oct 2005.
- [17] U. Scheuermann, U. Schilling, "Cosmic Ray Failures of Power Modules – The Diode Makes the Difference," *Proc. of PCIM' 2015*, 2015.
- [18] M. Ciappa, "Selected failure mechanisms of modern power modules," *Microelectronics reliability* vol.42, no.4, pp. 653-667, 2002.
- [19] M. Musallam, C.M. Johnson, "An Efficient Implementation of the Rainflow Counting Algorithm for Life Consumption Estimation," *IEEE Transactions on Reliability*, vol.61, no.4, pp.978-986, Dec. 2012.
- [20] M. Held, P. Jacob, G. Nicoletti, P. Scacco, M.H. Poech, "Fast power cycling test of IGBT modules in traction application." *Proceedings of Power Electronics and Drive Systems, 1997 International Conference on*. Vol. 1. IEEE, 1997.
- [21] S. Holm, J. de Mare, "A simple model for fatigue life," *IEEE Transactions on Reliability*, vol.37, no.3, pp.314-322, Aug 1988.
- [22] D. Sera, R. Teodorescu, J. Hantschel, M. Knoll, "Optimized Maximum Power Point Tracker for fast changing environmental conditions," *IEEE International Symposium on Industrial Electronics, ISIE*, pp.2401-2407, 2008.
- [23] A. Andreas, T. Stoffel, NREL Solar Radiation Research Laboratory (SRRL): Baseline Measurement System (BMS); Golden, Colorado (Data); NREL Report No. DA-5500-56488, 1981.
- [24] R. Bründlinger, N. Henze, H. Hüberlin, B. Burger, A. Bergmann, F. Baumgartner, "prEN 50530–The New European Standard for Performance Characterisation of PV Inverters." *Proc. 24th European Photovoltaic Solar Energy Conf.* 2009.